Distribution of iron in multicrystalline silicon ingots

R. Kvande,[1,a)] L. J. Geerligs,[2] G. Coletti,[2] L. Arnberg,[1] M. Di Sabatino,[3] E. J. Øvrelid,[3] and C. C. Swanson[4]
[1]*Norwegian University of Science and Technology, Alfred Getz vei 2, N-7491 Trondheim, Norway*
[2]*ECN Solar Energy, P.O. Box 1, NL-1755 ZG Petten, The Netherlands*
[3]*SINTEF Materials and Chemistry, Alfred Getz vei 2, N-7465 Trondheim, Norway*
[4]*Eastman Kodak Company, Rochester, New York 14650-2155, USA*

(Received 1 February 2008; accepted 13 May 2008; published online 17 September 2008)

The distribution of iron in multicrystalline silicon ingots for solar cells has been studied. A *p*- and a *n*-type multicrystalline ingot were intentionally contaminated by adding 53 ppm wt (μg/g) of iron to the silicon feedstock and compared to a reference *p*-type ingot produced from ultrapure silicon feedstock. The vertical total iron distribution was determined by neutron activation analysis and glow discharge mass spectrometry. For the intentionally Fe-contaminated ingots, the distribution can be described by Scheil's equation with an effective distribution coefficient of 2×10^{-5}. The interstitial iron concentration was measured in the *p*-type ingots. In the Fe-contaminated ingot, it is almost constant throughout the ingot and constitutes about 50% of the total concentration, which is in conflict with the previous studies. Gettering had a large impact on the interstitial iron levels by reducing the concentration by two orders of magnitude. Considerable trapping was observed at crystal defects on as-cut wafers from the same ingot. The trapping was suppressed by gettering. The back diffusion of iron from the ingot top after complete solidification was modeled and found to affect the iron concentration up to a distance of approximately 17 mm into the ingot. The interstitial as well as the total iron concentration of the reference ingot were extremely low and difficult to measure accurately. © *2008 American Institute of Physics*. [DOI: 10.1063/1.2956697]

I. INTRODUCTION

Iron is considered to be one of the most common and harmful impurities present in *p*-type multicrystalline silicon (mc-Si) for use in solar cells. With its large capture cross section for electrons and deep level in the band gap, interstitial iron is known to reduce the minority carrier lifetime by creating recombination centers. Contamination sources during crystal growth are feedstock and furnace environment in addition to surfaces which are in direct contact with the melt/solidified silicon (i.e., crucible walls and silicon nitride lining).[1–4] Iron is also introduced during high temperature cell processing steps (emitter diffusion and firing of contacts). Concentrations in the range of 10^{14}–10^{15} cm^{-3} have been reported in commercial mc-Si ingots.[5,6] This is well above the concentration levels where *interstitial* iron could drastically reduce the solar cell performance.

As iron has a low distribution coefficient in silicon, most of the iron existing in the melt will accumulate in the liquid phase during crystal growth and be localized at the top of the solidified ingot. The solidification step therefore serves as an effective method for refining silicon. However, interstitial iron has a high diffusivity in solid silicon and iron accumulated at the top will diffuse back into the bulk during slow cooling from high temperatures.

The fact that interstitial iron is a fast diffuser in silicon makes it an element that is easy to getter during diffusion of the phosphorus emitter. Iron precipitated at defects (e.g., grain boundaries, dislocations, and oxygen precipitates) is, on the other hand, more difficult to getter due to high binding energies.[7] The kinetics for precipitated iron, especially for larger precipitates, to dissolve and diffuse to the gettering layer is too slow to remove iron completely from the bulk of the wafers. The precipitates may instead act as impurity sources, leaking iron into the silicon during high temperature processing steps. The *total* iron concentration is therefore not the sole parameter that needs to be taken into consideration when assessing the impact of iron on solar cell properties as also the *chemical state* will be of importance.

Mechanisms responsible for the distribution of iron through an ingot and for the distribution between precipitated and interstitial iron are quite diverse and still uncertain in their effects. The intention of the present study was to provide precise data to elucidate further those mechanisms by investigating ingots with known amounts of iron in the melt before crystallization.

In this paper, the iron distribution in mc-Si ingots grown by directional solidification in a pilot-scale furnace was determined by different characterization techniques. A known amount of iron was added to the silicon charge before melting which was incorporated in the ingot during growth. Chemical analysis techniques used for the investigations were neutron activation analysis (NAA) and glow discharge mass spectrometry (GDMS) which can quantify total element concentrations down to the parts per 10^9 level. The iron concentration in commercial mc-Si ingots has been previously studied by Istratov *et al.*[5] and Macdonald *et al.*[6] In the work presented here, however, the iron concentration in the feedstock was known, which made it possible to fit the iron

a)Electronic mail: rannveig.kvande@material.ntnu.no.

distribution, as expressed by Scheil's equation, to the measured values and in this way determine the effective distribution coefficient in mc-Si ingots.

To investigate how much of the iron existed in a dissolved state and how much was precipitated, the interstitial iron (Fe_i) concentration was measured by the change in minority carrier lifetime before and after FeB pair dissociation. The effect of gettering on the interstitial iron concentration was also investigated using the same technique. With accurate knowledge of Fe content in feedstock, in ingot, and the dissolved versus precipitated fractions, this study provides important information for understanding the precipitation behavior of iron during solidification and cooling.

The solidification experiments were conducted in a furnace which has been studied extensively during the past years.[8–10] The temperature of the top of the solidified ingot during cooling could therefore be estimated with high accuracy in order to model the back diffusion of iron from the ingot top into the bulk. This is relevant for achieving a better understanding of the poor quality areas of normal (not intentionally contaminated) ingots, and thus for yield and performance of those ingots.

The impact of high iron levels on minority carrier lifetime and solar cell performance will be fully reported in a separate paper.[45] Some of the main observations of that work were the considerably higher lifetimes measured on as-cut wafers from the *n*-type ingot and a prominent positive impact of solar cell processing on wafers from the *p*-type ingot. It was demonstrated that in the central part of the *p*-type Fe-contaminated ingot, cell efficiencies comparable to a *p*-type standard ingot without Fe additions were obtained.

II. INGOT GROWTH PROCEDURE AND SAMPLE PREPARATION

The solidification experiments were conducted in a Crystalox DS 250 pilot-scale furnace designed to solidify mc-Si ingots representative of those grown in the industry. The ingots were solidified vertically from the bottom with a planar solid-liquid interface. Heat was transferred to the silicon charge from the sides and all heat was extracted through the crucible bottom during crystal growth by controlled exposure to a water-cooled copper plate below the crucible. The cylindrical crucible was rotated during the experiments to assure complete symmetry in the ingots.

Three silicon ingots were produced, each having a weight of 12 kg, a diameter of 250 mm, and a height of 110 mm. Two ingots, one *p*-type and one *n*-type, were grown with addition of 53 ppm wt $(1.3\times10^{18}\ \mathrm{cm^{-3}})$ electrolytic high purity iron to the silicon charge before melting. A *p*-type reference ingot without iron addition was also grown in order to define the iron content in a standard material.

In all solidification experiments, high purity crucibles from Saint-Gobain Quartz (C10) made of synthetic fused silica containing 0.5 ppm wt iron[11] were used. The crucibles were coated with silicon nitride from UBE which had been purified in an acidic solution consisting of HF and HCl. After the cleaning process, the silicon nitride contained approximately 1 ppm wt Fe.[2] High purity solar grade silicon was used as feedstock, containing iron in the parts per 10^9 range. The *p*-type ingots were boron doped to give a resistivity of 1.1 Ω cm $(1.3\times10^{16}\ \mathrm{cm^{-3}})$ in the middle of ingot heights, as confirmed by four point probe measurements. The *n*-type ingot was doped with phosphorus, giving an average resistivity of 0.65 Ω cm $(7.8\times10^{15}\ \mathrm{cm^{-3}})$.

The center $125\times125\ \mathrm{mm^2}$ brick of each ingot was sliced into 240 μm thick wafers. The bottom and top of the bricks, having a thickness of about 4 mm each, were removed before wafering. Samples for NAA and GDMS measurements were cut adjacent to the bricks but on opposite sides and were located at sufficient distances from the ingot sides to avoid contamination from crucible and lining.

The samples for GDMS analyses, having a size of $30\times30\ \mathrm{mm^2}$ and a thickness of 10 mm in ingot height direction, were ground on 120 grit SiC paper to assure a planar surface, and were cleaned in ethanol. The samples for NAA were $20\times80\ \mathrm{mm^2}$ and had a thickness of 3 mm. To avoid surface contamination, the latter samples were carefully cleaned in a chemical etch before the measurements.

The minority carrier lifetime was measured by quasi-steady state photoconductance (QSSPC).[13] Lifetimes were measured on "as-cut" wafers which had been etched to remove saw damage and cleaned before being surface passivated on both sides by deposition of silicon nitride films using plasma-enhanced chemical vapor deposition. In addition, lifetime was measured on wafers which had been gettered by diffusing phosphorus into the wafers in a belt furnace and thereafter surface passivated (the emitter was removed by etching). The gettered wafers were located adjacent to the as-cut wafers, assuring comparable crystal structures and impurity concentrations.

III. CHEMICAL ANALYSIS PROCEDURES

GDMS is a technique that allows quantitative chemical analysis of elements present in solar cell silicon (e.g., Ref. 14). The sputtered sample area was approximately 50 $\mathrm{mm^2}$ and the depth removed was approximately 0.5 μm. The sputtering rate for Si materials is 20 nm/s. The analyzed area was presputtered for about 10 min in order to remove surface contamination.

The samples for NAA were irradiated at the Missouri State University with a thermal neutron flux of $2\times10^{12}\ \mathrm{cm^{-2}\,s^{-1}}$ for 75 h. Further analyses were conducted at the Kodak Eastman research laboratory where gamma rays emitted from the samples were counted in order to determine the iron concentrations. The lowest Fe levels detected in the silicon matrix were $9\times10^{12}\ \mathrm{cm^{-3}}$.

The interstitial iron concentration was studied by dissociating FeB pairs by illuminating the wafers.[15] This is a well-established and very sensitive method to determine Fe_i where the change in minority carrier lifetime caused by the illumination is assumed to be directly related to the Fe_i concentration. Fe_i levels as low as $10^{10}\ \mathrm{cm^{-3}}$ can be calculated by this method.[16] Although measurements on mc-Si are not exactly quantitative, deviations are moderate.[17]

Illumination from a halogen lamp with an intensity of approximately 0.1 W $\mathrm{cm^{-2}}$ was used to dissociate the FeB

pairs. The wafers were clamped to a cooled Al block during illumination to avoid heating and too much repairing. Wafers from the *p*-type Fe-contaminated ingot were illuminated for 60 s. Some of these samples were also illuminated for increasing periods of time where no change in lifetime was observed, indicating that 60 s illumination was enough to achieve complete dissociation. Wafers from the *p*-type reference ingot experienced lifetime degradation when illuminated for 60 s (presumably due to creation of a Boron-Oxygen-related defect, as discussed in Sec. IV B). A shorter illumination time was therefore employed for these wafers (20 s was typically sufficient to obtain complete dissociation). However, due to the sensitivity of illumination time, a significant error still remained for these latter measurements. All lifetime measurements were performed 20 s after illumination, limiting repairing to a negligible level of 1%.[15]

Trapping[18] along crystal defects was established by using a combination of microwave photoconductance decay[19] (μW-PCD) and modulated free carrier absorption (MFCA).[20] The former lifetime technique has a resolution of 0.25 mm and a bias of 2 suns was used, while the latter has a resolution of 0.125 mm and provides an intensity of about 30 suns. The QSSPC measurements show that above ~10 suns, trapping is no longer dominant as all the traps are filled (this illumination threshold will depend on the lifetime and the traps).

IV. RESULTS AND DISCUSSIONS

Performing solidification experiments in a pilot-scale furnace compared to industrial large-scale furnaces has the drawback of introducing uncertainties as to whether the results are applicable for commercial ingots. An uncertainty factor is the cooling rate after solidification which may not be identical in the laboratory-scale furnace (approximately 2.5 °C/min at higher temperatures) compared to industrial cases. This will influence the diffusion length of impurities during cooling. Also, due to a large contact surface toward possible contamination sources (i.e., crucible and silicon nitride lining) compared to ingot volume, the "red zone" will constitute a considerable share of a laboratory-scale ingot. The red zone is a denotation used for the outer parts of silicon ingots which are adjacent to crucible and top surface and hence experience low lifetimes. The extent of the red zone was reduced in these experiments by using high purity crucibles containing iron levels approximately 60 times lower than what is commonly found in standard crucibles (Vesuvius solar crucible). Moreover, the purified silicon nitride contained iron levels 20 times less than what is commonly found in standard (uncleaned) silicon nitride. In addition to reducing the impact of the red zone, using high purity crucibles and coating also had the advantage of providing a better control of iron contamination from the surroundings during the experiments. Despite these differences between laboratory-scale experiments and industrial conditions, it is believed that the main results are representative for commercial ingots.

The level of 53 ppm wt of Fe in the silicon feedstock was estimated to be necessary to obtain sufficient iron incorporation in the solid phase for noticeable effects which could be accurately measured. In particular, it would result in iron concentrations close to the ingot tops which could more easily be detected by NAA and GDMS. When studying the growth morphology of the two solidified ingots with Fe additions, it was observed that the planar front had been maintained during crystallization and that only the last remaining melt had solidified by dendritic growth, as shown in Fig. 1. The center of the ingots solidified first, still being able to maintain a planar growth.

FIG. 1. Pictures taken from the top of the *p*-type Fe-contaminated ingot showing dendrites (left) and the reference ingot showing carbide particles (right).

Selected regions of the ingots were analyzed using electron microprobe. Particles at the top of the Fe-contaminated ingots were found to exist as $FeSi_2$ with a diameter as large as 10 μm. The particle density was, in average, 1 mm^{-2} in the studied areas. No particles could be detected at the top of the noncontaminated ingot or in the central parts of any of the ingots.

For the reference ingot, direct contact between ingot and crucible was observed in some regions. This resulted in increased oxygen levels, as measured by Fourier transform infrared spectroscopy according to ASTM standards,[21] showing an interstitial oxygen (O_i) concentration of 4.2×10^{17} cm^{-3} in the middle of ingot height with decreasing trend toward the top. The O_i concentrations in the central parts of the *p*- and *n*-type ingots with Fe additions were 1.5×10^{17} and 2.5×10^{17} cm^{-3}, respectively. The oxygen was more uniformly distributed in these ingots, showing an almost constant concentration level throughout the ingots. The O_i levels measured in the Fe-contaminated ingots are representative of what is commonly found in commercial ingots, where values around 2×10^{17} cm^{-3} in the middle of ingot heights have been reported.[22]

A. Total iron concentration

The total iron concentration in the *p*- and *n*-type ingots with Fe additions were measured by GDMS at increasing height from the ingot bottom, as shown in Fig. 2. The concentrations in the bulk of the reference ingot were below the detection limit and, therefore, only Fe concentrations at the top of this ingot are included in Fig. 2. Measurements were conducted on samples having the analyzed region in horizontal direction ("hori" in Fig. 2), meaning that the sputtered area was located parallel to the solidification front. In addition some vertical measurements ("vert" in Fig. 2) were performed on samples from the *p*-type Fe-contaminated ingot, where the analyzed area was located parallel to the growth direction. The size of the sputtered area was approximately 8 mm in diameter which caused some averaging to take

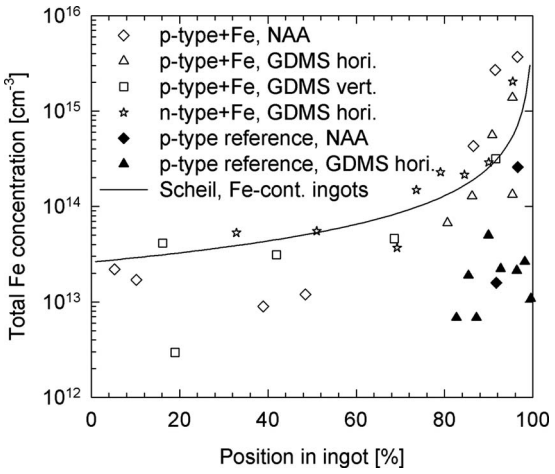

FIG. 2. Iron concentrations as determined by GDMS, NAA, and calculated from Scheil's equation using k_{eff} equal to 2×10^{-5}. 0% is the bottom and 100% the top of the ingots. The GDMS analyses had an accuracy of $\pm25-30\%$ and the NAA measurements of $\pm15\%$.

place in the vertical measurements. This effect was small as long as the measurements were performed at an adequate distance from the top, avoiding the region where the concentration increased very rapidly.

The iron distribution in the reference and *p*-type Fe-contaminated ingot was also determined by NAA at increasing vertical positions. The results are included in Fig. 2. The iron levels in the reference could only be detected close to the top where the concentrations were above the detection limits. Measurements of lateral variations of iron in the ingots were not performed.

Scheil's equation is used to describe the impurity concentration in solid phase C_s as a function of fraction solidified f_s, assuming no diffusion in solid phase and complete diffusion in liquid phase[23]

$$C_s = kC_0(1-f_s)^{(k-1)}, \tag{1}$$

where C_0 is the element concentration in the melt before solidification is initiated and k is the distribution coefficient, defined as the concentration in solid divided by the concentration in bulk liquid. A boundary layer will be present in the melt in front of the solidifying interface due to incomplete mixing, causing an enrichment of iron in this region. Therefore, k will be an *effective* distribution coefficient k_{eff}, which is influenced by the growth conditions and is given by

$$k_{\text{eff}} = \frac{k_0}{k_0 + (1-k_0)e^{-(v\delta/D_l)}} \tag{2}$$

where v is the growth rate, δ, is the thickness of the boundary layer, D_l is the diffusion coefficient in the melt, and k_0 is the distribution coefficient as given by the equilibrium phase diagram.

The iron distribution, as given by Scheil's equation, is included in Fig. 2, giving the best fit to the measured values by using an effective distribution coefficient of 2×10^{-5}. Values close to top were not included in the calculation of k_{eff} as they were influenced by back diffusion after completion of solidification (this back diffusion extends over a distance of approximately 17 mm, as shown in Sec. V). In fitting k_{eff}, it was assumed that all iron existing in the melt originated from the added iron and that contributions from other sources were so small by comparison that they could be neglected (i.e., $C_0=53$ ppm wt).

TABLE I. Values used for calculating the boundary layer thickness.

Constant	Value	Reference
k_0	8×10^{-6}	26
D_l	4×10^{-4} cm^2/s	8
v	4×10^{-4} cm/s	27

The value of k_{eff} is much more precise than earlier reported (<0.05).[6] The fact that k_{eff} is close to the equilibrium value (given in Table I) may indicate that enhanced Fe incorporation due to a "segregation mechanism" is not taking place to same degree as previously assumed. The segregation mechanism is suggested to deplete the iron existing in the solid phase close to the solid-liquid interface due to segregation of iron to extrinsic defects, increasing the incorporation from the melt.[6]

The boundary layer thickness in front of the solid-liquid interface was found to be 9 mm, as calculated from Eq. (2), where values for k_0 and D_l are given in literature and v has been determined experimentally in separate experiments (Table I). The thickness of the boundary layer in *monocrystalline* silicon grown by the Czochralski method has been reported to be approximately 0.6 mm at low crystal rotation velocity (5 rpm).[24] However, this value is not representative for directional solidification as the boundary layer is known to be thicker in this solidification method compared to the Czochralski process.[25]

Macdonald *et al.*[6] reported iron concentrations of approximately 6×10^{13} cm^{-3} in a commercial ingot at 60% of ingot height, similar to the levels we find in ingots contaminated with 53 ppm wt iron. By assuming that a k_{eff} of 2×10^{-5}, as determined in this work, also applies for the commercial ingot, the initial iron concentration calculated from Scheil's equation ($C_0\approx0.4C_sk_{\text{eff}}^{-1}$) is found to be 1.2×10^{18} cm^{-3} (48 ppm wt). It seems unrealistic that contamination from feedstock, contact surfaces, and furnace environment can cause such a high level. This indicates that results obtained from chemical analysis at these low iron concentrations should be interpreted with caution. This is emphasized by the observation that toward the top the difference between the two ingots increases: the iron concentration in the ingot contaminated with 53 ppm wt increases more than that in the commercial ingot. However, since the iron measurements at the top are affected by solid state back diffusion (see Sec. V), it is not trivial to use the measurements at the top to estimate the initial concentration of iron in the melt.

For the *p*-type reference ingot produced in this work, only Fe concentrations in the top of the ingot could be detected. In this region, the values are influenced by back diffusion and the iron concentration in the melt before solidification could therefore not be determined.

B. Interstitial iron concentration

The interstitial iron concentration was determined from the change in minority carrier lifetime by illumination of the

sample. If also other processes than the FeB dissociation are affected by illumination, such as formation of boron-oxygen complexes[28] or breaking of Cu–Cu pairs,[29] the Fe_i concentration cannot be detected by using this technique. As the *p*-type reference ingot contained relatively high oxygen levels and high lifetimes, two opposite trends were found to be significant for longer illumination times (approximately 40 s illumination) at an injection level of 1×10^{15} cm^{-3}, namely, (i) dissociation of FeB pairs, which increased the minority carrier lifetime, and (ii) formation of boron-oxygen related defects which reduced the lifetime.

Evaluating the crossover point is a method used to identify whether the change in minority carrier lifetime caused by illumination actually is linked to the dissociation of FeB pairs. The crossover point is defined as the excess carrier density Δn at which the minority carrier lifetime remains, unchanged before and after illumination when transforming FeB pairs to Fe_i.[30] The position of the crossover point is doping dependent and has been determined by Macdonald *et al.*[31] For the *p*-type Fe-contaminated ingot, the crossover point varied from 1.2×10^{14} to 2.2×10^{14} cm^{-3}, which is close to the value reported in literature ($\sim2\times10^{14}$ cm^{-3}) for the existing boron concentrations. For the *p*-type reference, the crossover point was difficult to detect accurately as the lifetime curves before and after illumination were closely located.

Wafers from the *p*-type Fe-contaminated ingot had very low lifetimes and hence carrier diffusion lengths less than the thickness of the wafers. Since generation is rather shallow (i.e., at the top of the wafer, near the surface) in the QSSPC technique, for low lifetimes the actual injection level during the measurements was approximated by replacing the wafer thickness with two times the diffusion length $[L=(D\tau)^{1/2}]$,[31] using a minority carrier diffusion coefficient of 33.5 cm^2/s.[32]

In the *p*-type Fe-contaminated ingot, there is no reason to expect strong contamination with other impurities. Therefore, the observed lifetime in as-cut wafers of this ingot, between 0.7 and 2.1 μs, should be dominated by Fe_i and possibly Fe precipitates. Indeed, the interstitial iron concentrations measured by the pair-dissociation method can roughly (with an uncertainty of about a factor 2) account for the lifetime. This confirms that despite the very high Fe concentrations and low lifetimes, the pair dissociation method is quite accurate and enables correct measurements of the Fe_i concentrations.

The Fe_i concentrations vertically in the *p*-type Fe-contaminated ingot and the *p*-type reference are shown in Fig. 3. The Fe_i concentration was also measured on gettered wafers to evaluate the efficiency of the gettering to remove interstitial iron from the bulk of the wafers. The results are included in Fig. 3.

The interstitial iron distribution in the *p*-type reference shows a typical trend in the bottom and top on as-cut material. Here the concentration is higher at the bottom due to in-diffusion from crucible/lining and at the top due to segregation. In the bulk of the ingot Fe_i is relatively uniformly distributed. It should be kept in mind, however, that due to the very small amounts of iron present in the reference ingot, it was difficult to quantify the concentrations with high accuracy. The Fe_i levels (approximately 2×10^{10} cm^{-3} in the central part of the ingot) are unusually low compared to commercial ingots where concentrations are found to be a factor of 10 higher.[6,33] This indicates that the pure crucible and silicon nitride lining have contributed in producing mc-Si ingots low in iron, despite direct contact between ingot and crucible.

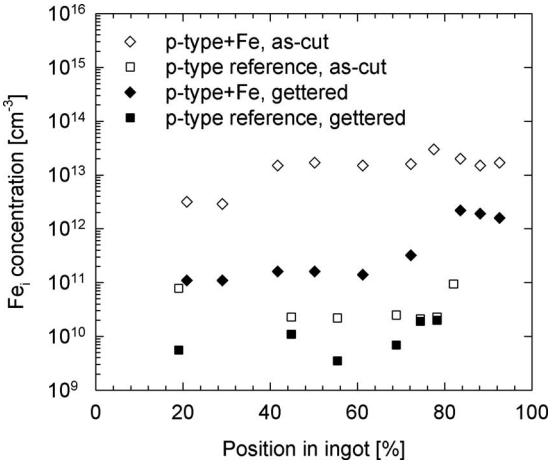

FIG. 3. Interstitial iron concentrations in as-cut and gettered wafers from both *p*-type ingots (Fe-contaminated and reference).

Except from close to the bottom, the interstitial iron concentrations vertically in the *p*-type Fe-contaminated ingot were approximately constant in as-cut material, showing an average of 2×10^{13} cm^{-3}. The almost constant Fe_i distribution in the bulk of both *p*-type ingots differs from investigations made by Macdonald *et al.*[6] where the interstitial iron concentrations were explained by a Scheil distribution.

Gettering had a major impact on the *p*-type Fe-contaminated ingot by reducing the Fe_i concentration to a level of approximately 1.5×10^{11} cm^{-3} in the bulk, as shown in Fig. 3. This value is in the same order of magnitude as Fe_i concentrations measured on gettered wafers from commercial ingots[34] and does not conflict with high efficiency cells (lifetime is not limited by Fe_i). The same prominent effect of the gettering was not observed for the *p*-type reference ingot which may be related to a less improvement potential due to the low iron levels already present in this ingot. It can also be a result of contamination from the environment or dissolution of iron precipitates during the high temperature gettering step, which may have a large effect at these low concentrations.

The lifetime due to the amount of Fe_i present in the *p*-type Fe-contaminated ingot after gettering would be approximately 500 μs. This value is much higher than the actual lifetime in this ingot. The gettering is therefore so effective that the lifetime is limited by other impurities and by crystal defects rather than by the doped Fe. Also, as will be shown in the next section, Fe precipitates do not seem to increase the activity of crystal defects in gettered samples, resulting in lifetimes which are almost comparable (around 50 μs) in the central part of the reference and *p*-type Fe-doped ingot.

The Fe_i concentration in the bulk of the *p*-type Fe-contaminated ingot constitutes approximately 50% of the to-

tal concentration. This share is reduced to some few percent close to the top. As there are no reliable data of the total iron concentration in the bulk of the reference ingot, no firm conclusions about the fraction precipitated iron in that material can be made. High Fe_i concentrations in mc-Si have also been reported in Fe-implanted wafers which were annealed at 900 °C and subsequently cooled to 650 °C at a cooling rate comparable to the situation that takes place during ingot cooling after solidification completion.[33] Surprisingly, all iron was found to remain interstitial at a concentration of 2×10^{13} cm^{-3}, which is the same level as obtained in this work. It was suggested that an energetic barrier is present at lower temperatures which prevents further precipitate formation and causes the high Fe_i concentrations. An interstitial iron concentration of 2×10^{13} cm^{-3} corresponds to the solubility limit of iron at 870 °C.[35] This temperature is located in a precipitation free regime according to Ramappa and Henley,[36,37] who found that iron precipitation will not take place between 760 and 920 °C. It was also reported, in the same investigations, that significant precipitation will occur in a temperature range of 400–800 °C. In this temperature regime, the most favorable precipitation conditions are believed to be present, where the supersaturation is sufficient high to create a large driving force for iron precipitation, while the diffusivity is high enough to enable iron to reach defects where it can precipitate. Our results cannot be explained by this latter finding, where no further precipitation seemed to have taken place in the *p*-type Fe-contaminated ingot during cooling from 870 °C.

Previously, it has been reported for nonintentionally Fe-doped ingots that more than 99% of all iron exists in a precipitated state.[6,38] The contradictory absence of such precipitation in our Fe-doped ingot cannot be explained by classic precipitation models. Alternative explanations could be a saturation of precipitated iron at crystal defects at high Fe concentrations which prevents further precipitation, or random differences in dislocation density and grain size between the studied ingots which affect the number of precipitation sites. However, given the results in the previous section, it is also possible that this strange discrepancy is *measurement* related. It may be questioned whether chemical analysis techniques such as NAA and GDMS are able to detect the small amounts of iron present in the central region of noncontaminated mc-Si ingots.

C. Trapping

Minority carrier trapping was observed by QSSPC in the *p*-type Fe-contaminated ingot, being especially pronounced in the bottom, probably due to high defect densities in this region, and in the top where segregation had resulted in high iron concentrations. The trapping density as function of ingot height is shown in Fig. 4. No or only very weak trapping was found in the *p*-type reference and *n*-type Fe-contaminated ingot.

Furthermore, in the *p*-type Fe-contaminated ingot, unusually strong trapping is observed on as-cut wafers using μW-PCD, appearing as fine structures in the lifetime maps. This is visible as a reversed contrast (areas affected by trapping seems to have high lifetime) in Fig. 5(a). Such fine structures with pronounced trapping mainly correlate with regions of high dislocation densities in addition to grain boundaries.[39]

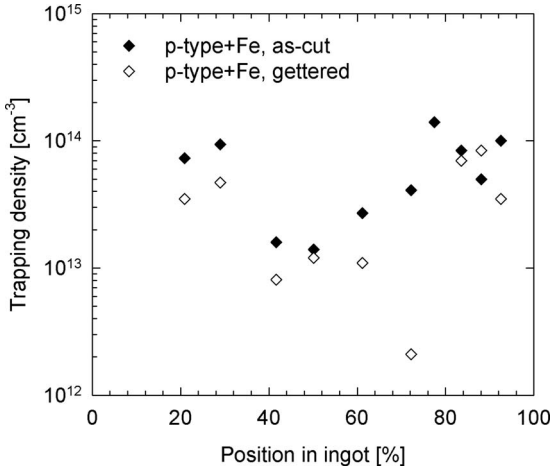

FIG. 4. Trapping density vertically in the *p*-type Fe-contaminated ingot, from QSSPC measurements.

The reference ingot did not show this trapping phenomenon, not even at the bottom of the ingot (which is contaminated by in-diffused Fe and other impurities). Clearly, the trapping is related to the iron doped into this ingot, showing that gettering can effectively remove significant amounts of iron from the crystal defects. It is expected that iron precipitates at crystal defects as $FeSi_2$.[40] This chemical state of iron is, however, known to introduce deep levels within the band gap[41] and should therefore create recombination centers and not contribute to the trapping. Macdonald *et al.* have suggested that boron-impurity pairs create trapping centers[42] which in this case would imply that iron is present in an interstitial state along the crystal defects in as-cut wafers.

V. BACK DIFFUSION

The concentration, chemical state, and location of impurities in mc-Si ingots are influenced by several phenomena as shown in Fig. 6. The main mechanisms affecting the iron concentration in mc-Si ingots are segregation, solid state indiffusion from crucible/lining, and back diffusion from ingot top into bulk during slow cooling from high temperatures.

Because of the high iron concentrations close to the top of the intentionally contaminated ingots, accurate measurements of Fe profiles are provided which give the opportunity of comparing models with measurements for the phenomenon of back diffusion. In this study the back diffusion of iron from the top of the *p*-type Fe-contaminated ingot was modeled using COMSOL Multiphysics.[43] The modeled Fe concentration was compared to the measured concentration profile in the affected region.

The diffusion in the solid phase can, in general, be described by Fick's second law by assuming a one dimensional vertical concentration gradient[44]

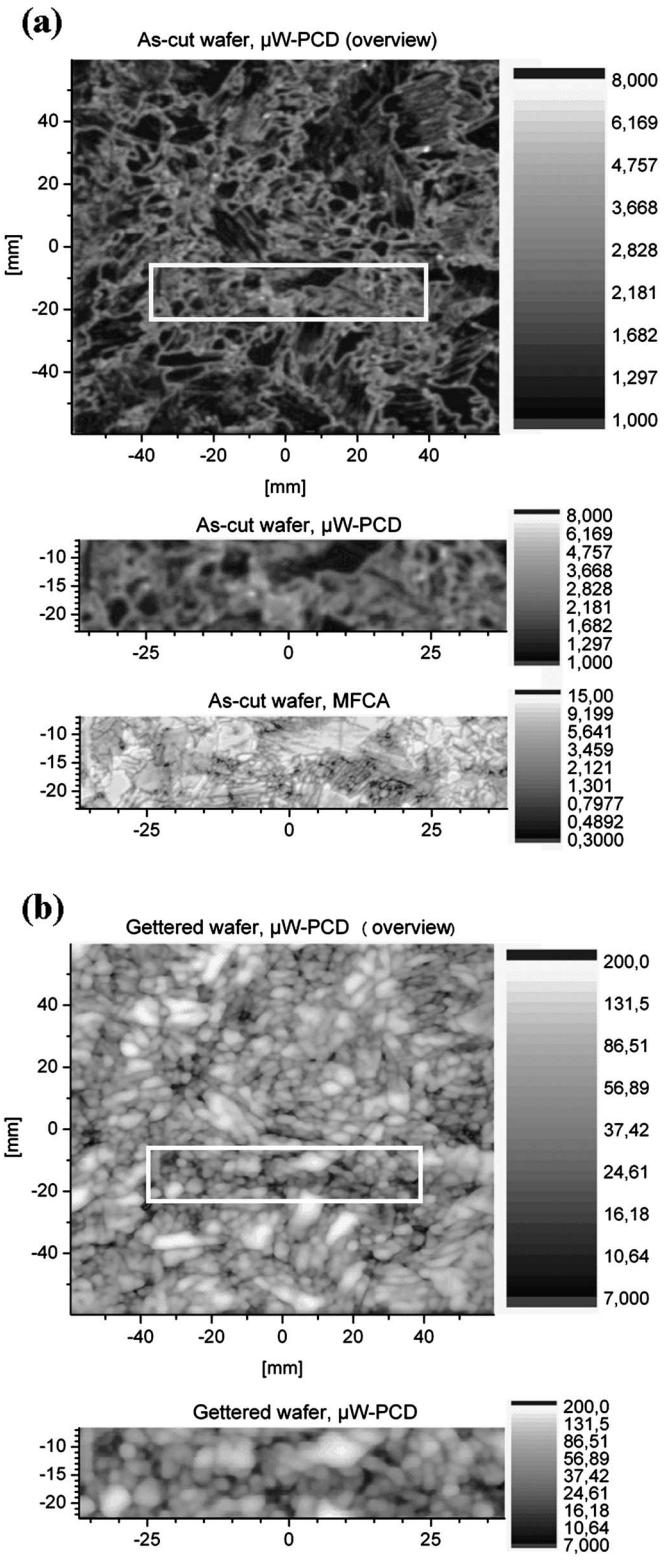

FIG. 5. Lifetime maps of an as-cut wafer (a) from the central part of the *p*-type Fe-contaminated ingot and a gettered wafer (b) neighboring the as-cut wafer. The lifetime was measured both by using μW-PCD at low injection level (sensitive to traps), and by MFCA at high enough injection level to be insensitive to traps (MFCA for comparison, only in the as-cut wafer). Note that the MFCA method has a higher measurement resolution and therefore shows a more detailed crystal defect structure. The MFCA lifetime is inaccurate, in this particular measurement, because of strong focusing of the generation laser which makes the usual mathematical analysis of the measurement invalid.

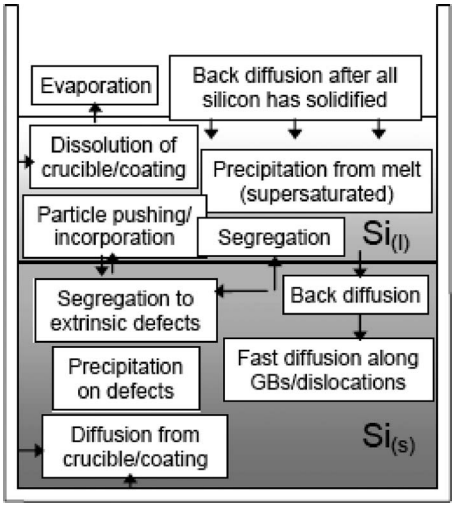

FIG. 6. Overview of some of the most important mechanisms affecting concentration, chemical state, and localization of impurities in mc-Si.

$$\frac{\partial C}{\partial t} = D\frac{\partial^2 C}{\partial x^2}. \tag{3}$$

To model the back diffusion after complete solidification, it was assumed that all iron had accumulated at the top of the ingot. The iron concentration below this heavily contaminated layer was small in comparison and was assumed to be zero before back diffusion was initiated. Iron started to diffuse back into the bulk at the moment when all silicon had solidified (i.e., $f_s = 1$). The Fe_i concentration in the uppermost layer during cooling was difficult to quantify as it depended on the decreasing solubility and diffusivity of iron and the number of sites where precipitation could take place. For simplicity, the Fe_i concentration at the top was set to be constant during cooling.

The diffusivity of iron in solid silicon is temperature dependent and can be expressed as[35]

$$D_{\mathrm{Fe}} = 1.0 \times 10^{-3} \exp\left(-\frac{0.67eV}{k_B T}\right) (\mathrm{cm}^2/\mathrm{s}), \tag{4}$$

where k_B is the Boltzmann constant. To determine the back diffusion, it was necessary to know the temperature profile at the top of the ingot during cooling. The temperature development in an ingot grown in the same solidification furnace has been investigated by Meese *et al.*,[9] where thermocouples were introduced into the melt at different positions from the crucible bottom during a solidification experiment. The uppermost thermocouple was located 15 mm from the ingot top and estimations were made to be able to quantify the temperature at the very top. Figure 7 shows the estimated temperature profile at the top of the ingot, the temperature measured in the susceptor placed outside the crucible, and the power during the experiment producing the *p*-type Fe-contaminated ingot. The plateau at 1535 °C was the melting segment while the solidification took place at slow cooling from 1470 °C. The end of solidification is identified by an increased power supply to compensate for the absent of heat of fusion.

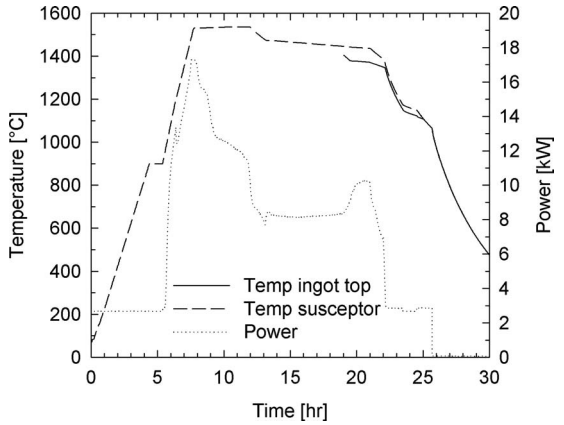

FIG. 7. Power and temperature profiles for the solidification experiment producing the *p*-type Fe-contaminated silicon ingot.

The result of the modeling of back diffusion is shown in Fig. 8 for different surface concentrations (i.e., iron concentrations at the top of the ingot). The measured values close to the ingot top are included in Fig. 8 for comparison. The back diffusion is found to affect the iron concentration up to a distance of approximately 17 mm into the ingot (to 85% of the ingot height). A concentration profile that gives good correlation with the measured values corresponds to a surface concentration of about 5×10^{15} cm^{-3}, equaling the solubility limit of iron at approximately 1140 °C.[35]

VI. CONCLUSIONS

Iron concentrations in multicrystalline silicon ingots produced from silicon feedstock doped with 53 ppm wt of Fe were measured from bottom to top using NAA and GDMS. The distribution could be explained by Scheil's equation using an effective distribution coefficient of 2×10^{-5}. This indicates that in these experiments a segregation mechanism proposed in earlier literature (segregation of iron to extrinsic defects close to the solid-liquid interface which increases the incorporation from the melt) gives at most a modest increase in the iron content. The total Fe concentrations measured in these Fe-doped ingots were similar to the total Fe concentrations reported in literature for commercial mc-Si ingots, indicating that the silicon feedstock used in these investigations was severely iron contaminated (which could also be a result of iron entering from the surroundings, i.e., crucible, lining, and furnace atmosphere) or that the measured iron concentrations are in error.

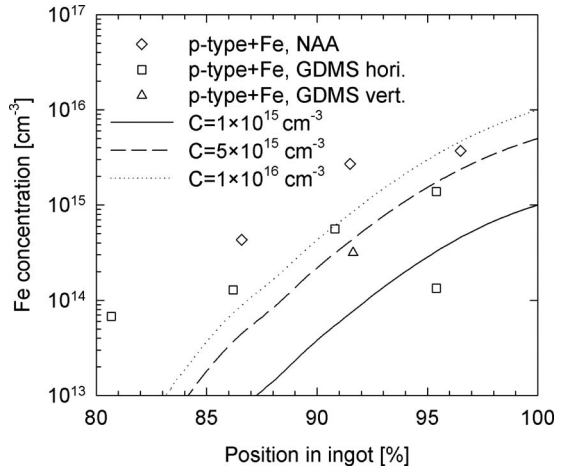

FIG. 8. Concentration profiles due to back diffusion close to the top of the *p*-type Fe-contaminated ingot for different surface concentrations. Measured values for this part of the ingot are included. The diffusivity was temperature dependent according to literature.

In the intentionally Fe-contaminated ingot the interstitial iron (Fe_i) concentration was almost constant at approximately 2×10^{13} cm^{-3}, which corresponds to about half of the total iron (except at the top). This ratio between precipitated and interstitial iron is surprisingly low, considering that previously about 99% of all iron has been reported to be noninterstitial for normal mc-Si ingots.

Gettering had a pronounced effect on the *p*-type Fe-contaminated ingot where the interstitial iron concentration was reduced by two orders of magnitude. Furthermore, the trapping at crystal defects was demonstrated to be high on as-cut wafers from this ingot. The trapping was suppressed by gettering which therefore apparently released iron from the defects. The Fe_i level in the noncontaminated ingot was already very low in as-cut wafers, and there was probably a slight reduction in the interstitial iron concentration by gettering.

Measurements and modeling of the back diffusion of iron from the ingot top after completed solidification are in relatively good agreement and show that the back diffusion extends over a distance of approximately 17 mm.

This work shows that when using a feedstock, which has been contaminated with 53 ppm wt iron, a large share of the iron appears to be present in a dissolved state. As interstitial iron can be well gettered, the high iron concentration in the feedstock does not seem to have a detrimental effect on the material quality after gettering for a large part of the ingot.

ACKNOWLEDGMENTS

Parts of this work have been funded by the project "Crystalline Silicon Solar Cells-Cost Reduction" with the following partners: NTNU, SINTEF, IFE, REC, Scanwafer, and Elkem Solar. Funding from the industrial partners and the Norwegian Research Council (Contract No. 153207/210) is greatly acknowledged. The European project "Foxy-Development of solar-grade silicon feedstock for crystalline wafers and cells by purification and crystallisation" (SES6-019811) is also gratefully acknowledged for financial support. The authors would like to thank the staff at ECN for technical assistance in the experiments. The content is the responsibility of the authors.

[1]T. Buonassisi, A. A. Istratov, M. D. Pickett, M. Heuer, J. P. Kalejs, G. Hahn, M. A. Marcus, B. Lai, Z. Cai, S. M. Heald, T. F. Ciszek, R. F. Clark, D. W. Cunningham, A. M. Gabor, R. Jonczyk, S. Narayanan, E. Sauar, and E. R. Weber, Prog. Photovoltaics **14**, 512 (2006).
[2]B. Geyer, G. Schwichtenberg, and A. Müller, Conference Record of the 31st IEEE Photovoltaic Specialists Conference, 2005 (unpublished), p. 1059.
[3]M. Rinio, C. Ballif, T. Buonassisi, and D. Borchert, Proceeding of the 19th European Photovoltaic Solar Energy Conference, 2004 (unpublished), p. 762.
[4]T. Buonassisi, A. A. Istratov, M. D. Pickett, J. P. Rakotoniaina, O. Breitenstein, M. A. Marcus, S. M. Heald, and E. R. Weber, J. Cryst. Growth **287**,

402 (2006).
[5]A. A. Istratov, T. Buonassisi, R. J. McDonald, A. R. Smith, R. Schindler, J. A. Rand, J. P. Kalejs, and E. R. Weber, J. Appl. Phys. **94**, 6552 (2003).
[6]D. Macdonald, A. Cuevas, A. Kinomura, Y. Nakano, and L. J. Geerligs, J. Appl. Phys. **97**, 033523 (2005).
[7]S. A. McHugo, A. C. Thompson, A. Mohammed, G. Lamble, I. Perichaud, S. Martinuzzi, M. Werner, M. Rinio, W. Koch, H. U. Hoefs, and C. Haessler, J. Appl. Phys. **89**, 4282 (2001).
[8]H. Laux, E. A. Meese, E. J. Øvrelid, and M. M'Hamdi, Proceedings of the 20th Photovoltaic Solar Energy Conference, 2005 (unpublished), p. 1090.
[9]E. A. Meese, E. J. Øvrelid, H. Laux, and M. M'Hamdi, Proceedings of the 19th Photovoltaic Solar Energy Conference, 2004 (unpublished), p. 793.
[10]E. A. Meese and A. Westermoen, Proceedings of the 22nd European Photovoltaic Solar Energy Conference, 2007 (unpublished), p. 1141.
[11]Data sheet, Saint-Gobain Quartz, C10.
[12]E. Olsen and E. J. Øvrelid, Prog. Photovoltaics **16**, 93 (2008).
[13]R. A. Sinton, A. Cuevas, and M. Stuckings, Conference Record of the 25th IEEE Photovoltaic Specialist Conference, 1996 (unpublished), p. 457.
[14]M. Di Sabatino, A. L. Dons, J. Hinrichs, O. Lohne, and L. Arnberg, Proceedings of the 22nd European Photovoltaic Solar Energy Conference, 2007 (unpublished), p. 271.
[15]G. Zoth and E. Bergholz, J. Appl. Phys. **67**, 6764 (1990).
[16]D. H. Macdonald, L. J. Geerligs, and A. Azzizi, J. Appl. Phys. **95**, 1021 (2004).
[17]L. J. Geerligs, G. Coletti, and D. Macdonald, Proceedings of the 21st European Photovoltaic Solar Energy Conference, 2006 (unpublished), p. 692.
[18]D. Macdonald and A. Cuevas, Appl. Phys. Lett. **74**, 1710 (1999).
[19]G. Citarella, S. von Aichberger, and M. Kunst, Mater. Sci. Eng., B **91–92**, 224 (2002).
[20]S. W. Glunz and W. Warta, J. Appl. Phys. **77**, 3243 (1995).
[21]ASTM standard, ASTM F1188-93a.
[22]D. H. Macdonald, L. J. Geerligs, and S. Riepe, Proceedings of the 13th Workshop on Crystalline Silicon Solar Cell Materials and Processes, 2003 (unpublished), p. 182.
[23]M. C. Flemings, *Solidification Processing* (McGraw-Hill, New York, 1974).
[24]H. Kodera, Jpn. J. Appl. Phys. **2**, 212 (1963).
[25]J. M. Kim and Y. K. Kim, Sol. Energy Mater. Sol. Cells **81**, 217 (2004).
[26]F. A. Trumbore, Bell Syst. Tech. J. **39**, 205 (1960).
[27]R. Kvande, Ø. Mjøs, and B. Ryningen, Mater. Sci. Eng., A **413–414**, 545 (2005).
[28]K. Bothe, R. Sinton, and J. Schmidt, Prog. Photovoltaics **13**, 287 (2005).
[29]W. B. Henley, D. A. Ramappa, and L. Jastrezbski, Appl. Phys. Lett. **74**, 278 (1999).
[30]J. E. Birkholz, K. Bothe, D. Macdonald, and J. Schmidt, J. Appl. Phys. **97**, 103708 (2005).
[31]D. Macdonald, T. Roth, P. N. K. Deenapanray, T. Trupke, and R. A. Bardos, Appl. Phys. Lett. **89**, 142107 (2006).
[32]ASTM standard, ASTM F1535-94.
[33]D. Macdonald, T. Roth, L. J. Geerligs, and A. Cuevas, 108–109, in *Proceedings of the 11th International Autumn Meeting, Gettering and Defect Engineering in Semiconductor Technology XI, Gadest, 2005* Diffuse 519 (2005).
[34]P. Manshanden and L. J. Geerligs, Sol. Energy Mater. Sol. Cells **90**, 998 (2006).
[35]A. A. Istratov, H. Hieslmair, and E. R. Weber, Appl. Phys. A: Mater. Sci. Process. **69**, 13 (1999).
[36]D. A. Ramappa and W. B. Henley, J. Electrochem. Soc. **144**, 4353 (1997).
[37]W. B. Henley and D. A. Ramappa, J. Appl. Phys. **82**, 589 (1997).
[38]A. Holt, E. Enebakk, and A. K. Søiland, Proceedings of the 22nd European Photovoltaic Solar Energy Conference, 2007 (unpublished), p. 1155.
[39]W. Warta, Phys. Status Solidi A **203**, 732 (2006).
[40]T. Buonassisi, A. A. Istratov, M. Heuer, M. A. Marcus, R. Jonczyk, J. Isenberg, B. Lai, Z. Cai, S. Heald, W. Warta, R. Schindler, G. Willeke, and E. R. Weber, J. Appl. Phys. **97**, 074901 (2005).
[41]E. K. Evangelou, G. E. Giakoumakis, and C. A. Dimitriadis, Solid State Commun. **80**, 309 (1993).
[42]D. Macdonald, M. Kerr, and A. Cuevas, Appl. Phys. Lett. **75**, 1571 (1999).
[43]COMSOL AB, COMSOL Multiphysics, Version 3.3.
[44]J. Cranck, *The Mathematics of Diffusion* (Oxford University Press, London, 1975).
[45]G. Coletti, "Effect of intentionally Fe-doped feedstock on multicrystalline silicon solar cell efficiency," J. Appl. Phys. (submitted).